Inorganic Chemistry

Article

pubs.acs.org/IC

Crystal Growth, Structural Characterization, and Magnetic Properties of New Uranium(IV) Containing Mixed Metal Oxalates: $Na_2U_2M(C_2O_4)_6(H_2O)_4$ (M = Mn^{2+}, Fe^{2+}, Co^{2+}, and Zn^{2+})

Jeongho Yeon,[†] Mark D. Smith,[†] Athena S. Sefat,[‡] and Hans-Conrad zur Loye*,[†]

[†]Department of Chemistry and Biochemistry, University of South Carolina, Columbia, South Carolina 29208, United States

[‡]Materials Science and Technology Division, Oak Ridge National Laboratory, Oak Ridge, Tennessee 37831, United States

Supporting Information

ABSTRACT: A series of new mixed-metal oxalates containing U^{4+} and divalent transition metal cations, $Na_2U_2M(C_2O_4)_6(H_2O)_4$ (M = Mn^{2+}, Fe^{2+}, Co^{2+}, and Zn^{2+}), were synthesized via a hydrothermal route and structurally characterized by single crystal X-ray diffraction. All of the materials are triclinic, with space group $P\bar{1}$. The three-dimensional structure of these isostructural uranates consists of oxalate bridged UO_{10} and MO_6 polyhedra. The U^{4+} cation is surrounded by five oxalate ligands, while the M^{2+} cations are bonded to two oxalate ligands and four water molecules. The magnetic susceptibility data of these mixed metal oxalates were measured as a function of temperature and result in a value of the effective magnetic moment of 3.50 μ_B for U^{4+} cation in the Zn member, while the total effective moment of the Mn^{2+}, Fe^{2+}, and Co^{2+} members are 6.01, 5.46, and 5.06 μ_B, respectively. For all materials, negative Weiss constants were observed revealing that the materials exhibited local antiferromagnetic interactions. The U^{4+} cation exhibits a singlet ground state at low temperature. The materials were further characterized by infrared, UV−vis reflectance spectroscopy, and thermal analysis.

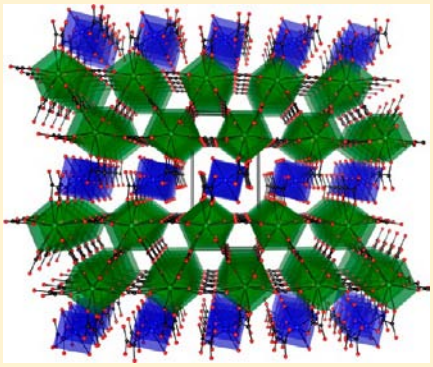

INTRODUCTION

The chemistry of uranium in extended structures has been extensively investigated due to its importance for long-term nuclear waste storage and for the development of fuel rod assemblies.[1−5] The majority of these efforts has focused on the most commonly found uranium species, the uranyl cation, UO_2^{2+}, which is usually observed in octahedral, pentagonal bipyramidal, or hexagonal bipyramidal coordination environments, and which typically exhibits two short and four or more longer bonds. Noticeably fewer investigations have focused on the chemistry of U^{4+}, perhaps in part due to the requirement that it has to be reacted under inert or reducing rather than ambient conditions that can be used for U^{6+} chemistry. The coordination environment of U^{4+} is quite different from that of U^{6+}, due to its significantly larger size (ionic radii, CN = 8; U^{6+} = 0.86 Å, U^{4+} = 1.00 Å),[6] which results in larger coordination environments, such as UO_8, UO_9, or UO_{10} polyhedra. Consequently, U^{4+} containing materials tend to exhibit extended structures quite different from those observed for related U^{6+} containing systems.

Another distinct difference between the U^{6+} and U^{4+} chemistry is that U^{4+} (f^2) contains two unpaired f-electrons that give rise to magnetic behavior, which is absent in the U^{6+} (f^0) species. To investigate the magnetic properties of U^{4+} containing materials, several groups have explored the preparation of U^{4+} containing oxides and have used high temperature, high pressure hydrothermal methods to prepare extended structures containing U^{4+}.[7−14] In particular the versatile germanate and silicate structures were targeted, as they are able to accommodate the large U^{4+} cation.[9,10,12] These hydrothermal reaction conditions are known to reduce U^{6+} to the +5 and +4 oxidation states, eliminating the need to start with a U^{4+} reagent. However, this can lead to mixed valent products.[8,9,11,13] Of additional interest, clearly, are U^{4+} based structures that contain a second metal that also has unpaired electrons, for example, a first row transitions element, to investigate potential magnetic interactions between the uranium-f and transition metal-d electrons.

To create U^{4+} containing extended structures, we pursued the preparation of mixed metal oxalates using uranium oxalate hexahydrate, $U(C_2O_4)_2(H_2O)_6$,[15] a convenient starting material that contains uranium in the +4 oxidation state. The +4 oxidation state can easily be maintained during synthesis, as the oxalate group creates a mild reducing solution environment at slightly elevated temperatures. Furthermore, it is well-known that the oxalate anion plays an important role in the separation and purification of actinide elements in general, due to its very prevalent chelating ability, where the oxalate group can be either terminally bidentate or act as a bridging tetradentate ligand.[16] This extensive chelating ability has led to a large collection of oxalate based framework structures containing a

Received: December 5, 2012
Published: February 1, 2013

   dx.doi.org/10.1021/ic3026733 | Inorg. Chem. 2013, 52, 2199−2207

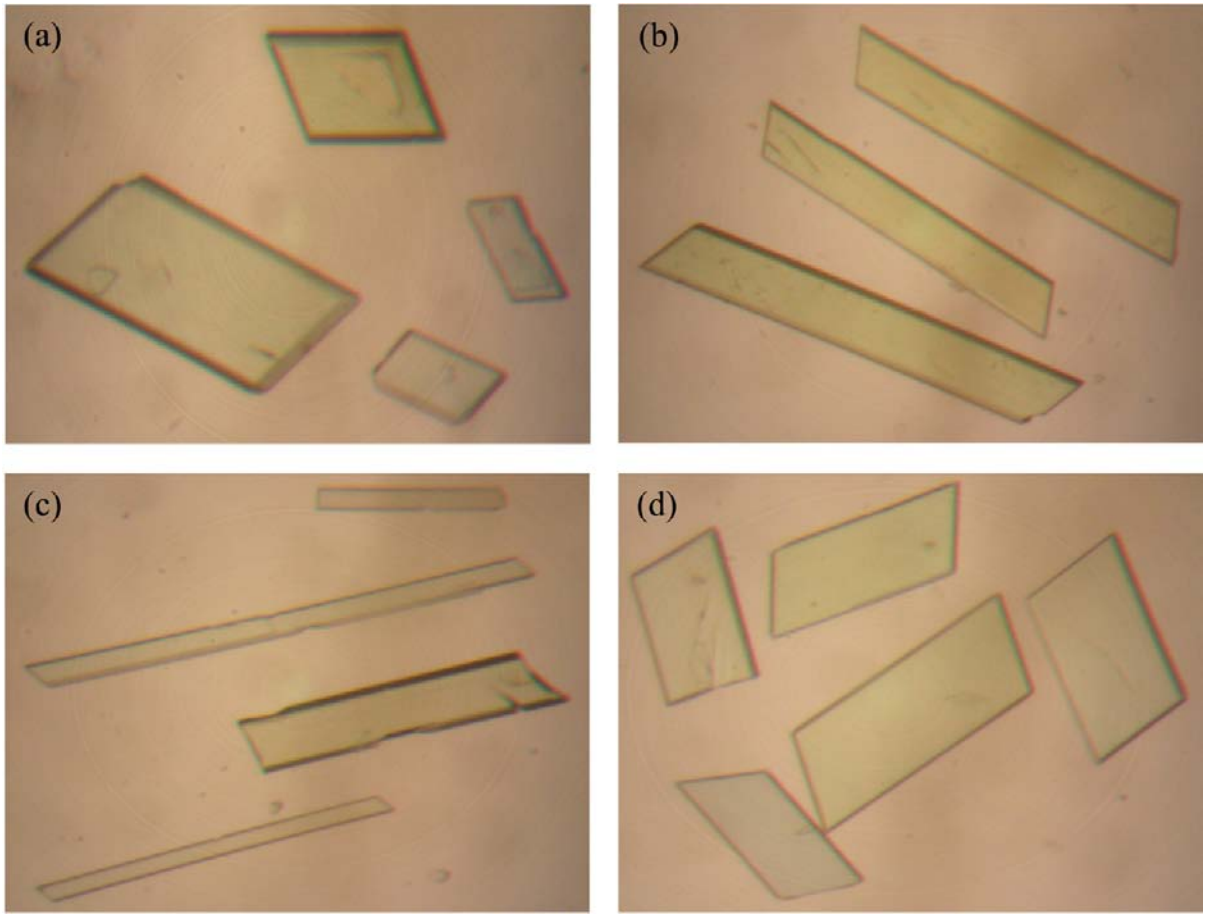

Figure 1. Photographic images of single crystals of (a) $Na_2U_2Mn(C_2O_4)_6(H_2O)_4$, (b) $Na_2U_2Fe(C_2O_4)_6(H_2O)_4$, (c) $Na_2U_2Co(C_2O_4)_6(H_2O)_4$, and (d) $Na_2U_2Zn(C_2O_4)_6(H_2O)_4$. The crystals are approximately 0.6 mm in length.

wide variety of metal cations, including molecular structures,[17,18] 1-D chain structures,[19,20] sheet structures,[21,22] as well as extended three-dimensional structures,[23,24] depending on the specific structure directing role of the oxalate groups in the material. In the case of uranium oxalates, a significant number of investigations have focused on U^{6+} containing materials, while only a very small number of U^{4+} containing oxalate structures with unique crystallographic sites have been reported. These include $(NH_4)_2U_2(C_2O_4)_5(H_2O)_{0.7}$,[23] $U(C_2O_4)_2(H_2O)_6$,[15] α- and β-$K_4U(C_2O_4)_4(H_2O)_4$,[25] α- and β-$U(C_2O_4)_2(H_2O)_2$,[26] $UF_3(C_2O_4)_{0.5}(H_2O)$,[27] $K_2UMn(C_2O_4)_4(H_2O)_9$,[24] $(C(NH_2)_3)_4U(C_2O_4)_4(H_2O)_2$,[16] $K_2U_2Mg_2(C_2O_4)_7(H_2O)_{11}$,[28] and $Ba_2U(C_2O_4)_4(H_2O)_8$.[29] Of these, $K_2UMn(C_2O_4)_4(H_2O)_9$ is the only mixed-metal system that includes a paramagnetic element (Mn^{2+}) other than the U^{4+} cation.

In this article, we report on the synthesis, characterization, and magnetic properties of a new series of U^{4+} containing mixed metal oxalates, $Na_2U_2M(C_2O_4)_6(H_2O)_4$ (M = Mn^{2+}, Fe^{2+}, Co^{2+}, and Zn^{2+}), representing rare examples of mixed-metal uranium oxalates containing two different magnetic cations.

EXPERIMENTAL SECTION

Reagents. $U(C_2O_4)_2(H_2O)_6$ was prepared from $UO_2(NO_3)_2(H_2O)_6$ (Fisher, ACS grade), $H_2C_2O_4{\cdot}2H_2O$ (Alfa Aesar, 98%), and $Na_2S_2O_7$ (Alfa Aesar, 85+%). Na_2CO_3 (Alfa Aesar, 99.5%), $MnCl_2{\cdot}4H_2O$ (Alfa Aesar, 99%), $FeCl_2{\cdot}4H_2O$ (Alfa Aesar, 98+%), $CoCl_2{\cdot}6H_2O$ (J.T. Baker, 99+%), $ZnCl_2$ (Alfa Aesar, 98+%), and $H_2C_2O_4{\cdot}2H_2O$ (Alfa Aesar, 98%) were used as received. ***Warning!*** *Although the uranium precursors used contain depleted uranium, standard safety measures for handling radioactive substance should be followed.*

Synthesis. Single crystals of the reported materials were grown via a hydrothermal route using $U(C_2O_4)_2(H_2O)_6$ as a U(IV) precursor. $U(C_2O_4)_2(H_2O)_6$ was synthesized using $UO_2(NO_3)_2{\cdot}6H_2O$, $Na_2S_2O_7$, $H_2C_2O_4{\cdot}2H_2O$, and HCl. A 2 mmol portion of $UO_2(NO_3)_2{\cdot}6H_2O$ was dissolved in dilute HCl (2 mL conc HCl and 18 mL of water) and warmed to 80 °C. A 4 mmol sample of $Na_2S_2O_7$ and 1 mL of conc HCl were added to the solution while stirring. The mixture was kept at 80 °C until the $UO_2(NO_3)_2{\cdot}6H_2O$ dissolved and was finally filtered to give a clear green solution. To this, a solution of $H_2C_2O_4{\cdot}2H_2O$ (3.6 mmol in 5 mL of water) was slowly added with stirring, causing a precipitate to form. The mixture was stirred for another 30 min, and the solid precipitate was filtered, washed with water and acetone, and dried at room temperature. The identity and phase purity of the $U(C_2O_4)_2(H_2O)_6$ product was confirmed by powder X-ray diffraction (see Figure S1).

For the preparation of $Na_2U_2M(C_2O_4)_6(H_2O)_4$ (M= Mn^{2+}, Fe^{2+}, and Co^{2+}), 0.4 mmol of $U(C_2O_4)_2(H_2O)_6$, 0.6 mmol of Na_2CO_3, 5 mmol of $H_2C_2O_4{\cdot}2H_2O$, and 6 mL of H_2O were combined with 0.2 mmol of $MnCl_2{\cdot}4H_2O$, $FeCl_2{\cdot}4H_2O$, and $CoCl_2{\cdot}6H_2O$, respectively.

For the preparation of $Na_2U_2Zn(C_2O_4)_6(H_2O)_4$, 0.4 mmol of $U(C_2O_4)_2(H_2O)_6$, 0.8 mmol of Na_2CO_3, 5 mmol of $H_2C_2O_4{\cdot}2H_2O$, and 6 mL of H_2O were combined with 0.2 mmol of $ZnCl_2$.

The respective solutions were placed into 23 mL Teflon–lined autoclaves. The autoclaves were closed, heated to 150 °C at a rate of 5 °C m^{-1}, held for 2 days, and cooled to room temperature at a rate of 6 °C h^{-1}. The mother liquor was decanted from the single crystal products, which were isolated by filtration and washed with distilled

dx.doi.org/10.1021/ic3026733 | Inorg. Chem. 2013, 52, 2199–2207

Table 1. Crystallographic Data for $Na_2U_2M(C_2O_4)_6(H_2O)_4$ (M = Mn^{2+}, Fe^{2+}, Co^{2+}, and Zn^{2+})

	$Na_2U_2Mn(C_2O_4)_6(H_2O)_4$	$Na_2U_2Fe(C_2O_4)_6(H_2O)_4$	$Na_2U_2Co(C_2O_4)_6(H_2O)_4$	$Na_2U_2Zn(C_2O_4)_6(H_2O)_4$
fw	1177.16	1178.07	1181.15	1187.59
cryst syst	triclinic	triclinic	triclinic	triclinic
space group	$P\bar{1}$ (No. 2)	$P\bar{1}$ (No. 2)	$P\bar{1}$ (No. 2)	$P\bar{1}$ (No. 2)
a (Å)	6.4556(5)	6.4504(7)	6.4419(1)	6.4418(2)
b (Å)	7.9032(6)	7.8759(8)	7.8595(1)	7.8671(2)
c (Å)	12.7572(9)	12.7802(13)	12.7780(2)	12.8053(4)
α (deg)	75.295(1)	75.622(2)	75.735(1)	75.622(1)
β (deg)	85.231(1)	85.269(2)	85.286(1)	85.185(1)
γ (deg)	68.820(1)	68.674(2)	68.464(1)	68.435(1)
V (Å^3)	587.00(8)	585.85(11)	583.206(15)	584.60(3)
Z	1	1	1	1
density (Mg/m^3)	3.330	3.339	3.363	3.373
abs coeff (mm^{-1})	14.464	14.573	14.728	15.009
cryst size (mm^3)	0.08 × 0.05 × 0.04	0.08 × 0.06 × 0.05	0.36 × 0.08 × 0.02	0.20 × 0.06 × 0.02
θ range	1.65−30.11	1.64−30.07	1.64−35.25	1.64−28.29
completeness to θ_{max}	99.2%	99.3%	99.2%	99.9%
R (int)	0.0600	0.0580	0.0509	0.0498
GOF (F^2)	1.020	0.974	1.018	1.045
$R(F)^a$	0.0318	0.0300	0.0320	0.0242
$R_w(F_o^2)^b$	0.0647	0.0584	0.0686	0.0540

$^a R(F) = \Sigma||F_o| - |F_c||/\Sigma|F_o|$. $^b R_w(F_o^2) = [\Sigma w(F_o^2 - F_c^2)^2/\Sigma w(F_o^2)^2]^{1/2}$.

Table 2. Selected Interatomic Distances (Å) for $Na_2U_2M(C_2O_4)_6(H_2O)_4$ (M = Mn^{2+}, Fe^{2+}, Co^{2+}, and Zn^{2+})

	$Na_2U_2Mn(C_2O_4)_6(H_2O)_4$	$Na_2U_2Fe(C_2O_4)_6(H_2O)_4$	$Na_2U_2Co(C_2O_4)_6(H_2O)_4$	$Na_2U_2Zn(C_2O_4)_6(H_2O)_4$
U(1)−O(6)	2.346(4)	2.348(4)	2.346(3)	2.352(3)
U(1)−O(5)	2.392(4)	2.395(4)	2.400(3)	2.387(3)
U(1)−O(9)	2.441(4)	2.439(4)	2.440(3)	2.445(3)
U(1)−O(11)	2.455(4)	2.458(4)	2.449(3)	2.455(3)
U(1)−O(12)	2.463(4)	2.475(4)	2.474(3)	2.473(4)
U(1)−O(10)	2.468(4)	2.473(4)	2.465(3)	2.472(3)
U(1)−O(1)	2.487(4)	2.496(4)	2.487(3)	2.492(3)
U(1)−O(4)	2.513(4)	2.511(4)	2.505(3)	2.511(3)
U(1)−O(2)	2.519(4)	2.513(4)	2.513(3)	2.515(3)
U(1)−O(3)	2.531(4)	2.528(4)	2.520(3)	2.518(3)
M(1)−O(7)	2.163(4)	2.132(4)	2.096(3)	2.065(3)
M(1)−O(7)	2.163(4)	2.132(4)	2.096(3)	2.065(3)
M(1)−O(14)	2.203(5)	2.133(5)	2.089(4)	2.112(4)
M(1)−O(14)	2.204(5)	2.134(5)	2.089(4)	2.112(4)
M(1)−O(13)	2.239(4)	2.181(5)	2.149(3)	2.181(4)
M(1)−O(13)	2.239(4)	2.181(5)	2.149(3)	2.181(4)

water and acetone. In all cases the reaction yielded a single phase product consisting of light green plate crystals in approximate 90% yield based on $U(C_2O_4)_2(H_2O)_6$. The addition of an excess of oxalic acid dihydrate is necessary to obtain high yield and high quality crystals (see Figure 1).

Single Crystal X-ray Diffraction. X-ray diffraction intensity data from plate crystals were measured at room temperature on a Bruker SMART APEX diffractometer (Mo Kα radiation, λ = 0.710 73 Å).[30] The raw area detector data frames were processed with SAINT+.[30] An absorption correction based on the redundancy of equivalent reflections was applied to the data with SADABS.[30] The reported unit cell parameters were determined by least-squares refinement of a large array of reflections taken from each data set (Table 1). Difference Fourier calculations and full-matrix least-squares refinement against F^2 were performed with SHELXTL.[31]

The four reported materials are isostructural and crystallize in the triclinic space group $P\bar{1}$ (No. 2), which was confirmed by the successful solution and refinement of the structures. The asymmetric unit consists of one uranium atom, one sodium atom, one divalent transition metal atom, two water molecules, two complete oxalate anions, and half each of two more oxalate ions located on inversion centers. The Mn, Fe, Co, and Zn atoms are also located on inversion centers. All non-hydrogen atoms were refined with anisotropic displacement parameters. After locating and refining all atoms anisotropically, the calculated electron density difference maps showed maxima corresponding to reasonable positions for water hydrogen atoms in the vicinity of oxygen atoms O13 and O14. These positions gave physically sensible water molecule and hydrogen bonding geometries. For refinement, O−H distances were restrained to d(O−H) = 0.84(2) Å, and H−H distances were restrained to be similar. All hydrogen atoms were assigned a common isotropic displacement parameter. Crystallographic data and selected interatomic distances are listed in Tables 1 and 2, respectively.

Powder X-ray Diffraction. Powder X-ray diffraction data were collected on a Rigaku D/Max-2100 powder X-ray diffractometer using Cu Kα radiation. The step-scan covered the angular range 5−70° 2θ in steps of 0.04°. No impurities were observed, and the calculated and experimental PXRD patterns are in excellent agreement (see Figure S2).

dx.doi.org/10.1021/ic3026733 | Inorg. Chem. 2013, 52, 2199−2207

Infrared Spectroscopy. IR spectra were recorded on a Perkin Elmer, Spectrum 100, FT-IR spectrometer in the 650−4000 cm^{-1} range.

UV−Vis Diffuse Reflectance Spectroscopy. Diffuse reflectance spectra of polycrystalline powder samples of the reported materials were obtained using a Perkin-Elmer Lambda 35 UV−vis scanning spectrophotometer equipped with an integrating sphere in the range 200−900 nm.

Thermal Analyses. Thermogravimetric analyses were carried out on a TA Instruments SDT Q600 simultaneous DTA-TGA by heating the single crystals at a rate of 10 °C/min under flowing N_2 and 5% H_2/N_2 gas up to a temperature of 900 °C.

Magnetic Property Measurements. The dc magnetization was measured as a function of temperature using a Quantum Design MPMS SQUID magnetometer. The polycrystalline samples were placed in a gelatin capsule, secured by a small amount of epoxy. For a typical temperature sweep experiment, the sample was cooled to 5 K under zero-field cooled (zfc) conditions, and data were collected by heating the sample from 5 to 350 K in an applied field of 1000 Oe. The sample was then cooled in the applied field (fc) to 5 K while data were collected.

RESULTS AND DISCUSSION

Synthesis. Hydrothermal methods are often used to generate U^{4+} in situ, enabling the researcher to start with a uranium source containing uranium is in its highest, U^{6+}, oxidation state. It is difficult to control the redox reaction, however, and hence mixed valent uranium containing products are often obtained. To eliminate the need for such a redox process, we synthesized the U^{4+} containing oxalate, $U(C_2O_4)_2(H_2O)_6$, in our laboratory using the method by Favas.[25] In addition, to maintain the uranium oxidation state during the reaction, we introduce an excess of oxalic acid to the reaction mixture. The oxalic acid stabilizes both the U^{4+} and the divalent transition metal cations in solution, creates a low pH environment, and is incorporated into the product. In the absence of the excess oxalic acid, the reactions generate extremely low yield, only poor quality crystals, and an unidentified powder impurity. In the presence of an excess oxalic acid, however, high quality single crystals of $Na_2U_2M(C_2O_4)_6(H_2O)_4$ (M = Mn^{2+}, Fe^{2+}, Co^{2+}, and Zn^{2+}), as shown in Figure 1, were obtained in essentially quantitative yield.

Structures. All members of the $Na_2U_2M(C_2O_4)_6(H_2O)_4$ (M = Mn^{2+}, Fe^{2+}, Co^{2+}, and Zn^{2+}) series crystallize in the triclinic space group $P\bar{1}$. The materials are isostructural and exhibit a three-dimensional structure consisting of UO_{10} and MO_6 (M = Mn^{2+}, Fe^{2+}, Co^{2+}, and Zn^{2+}) polyhedra bridged by oxalate, $C_2O_4^{2-}$, ligands. As shown in Figures 2 and 3, the layers of $U_2(C_2O_4)_6^{4-}$ in the *ab*-plane are connected by MO_6 octahedra along the *c*-axis resulting in a three-dimensional network. The Na atoms reside in the channels that run along the *a*-axis. Ten oxygen atoms from five oxalate ligands surround the crystallographically unique U^{4+} cations with U−O bond distances ranging from 2.346(4) to 2.531(4) Å. Of these five oxalate ligands, four are further linked to four additional U^{4+} cations and one is bonded to one M^{2+} (M = Mn, Fe, Co, and Zn) cation. The coordination environment of the U^{4+} cations, UO_{10}, is consistent with previously reported U^{4+} containing oxalates, and the U−O bond lengths are consistent with the average bond length of 2.479 Å for known materials.[16,21,25,28] The unique divalent cations are found in a nearly regular octahedron with the M−O bond distances ranging from 2.065(3) to 2.239(4) Å. In this octahedron, four of the oxygen ligands are water molecules, while the other two belong to two oxalates that connect to both M^{2+} and U^{4+} cations. The sodium

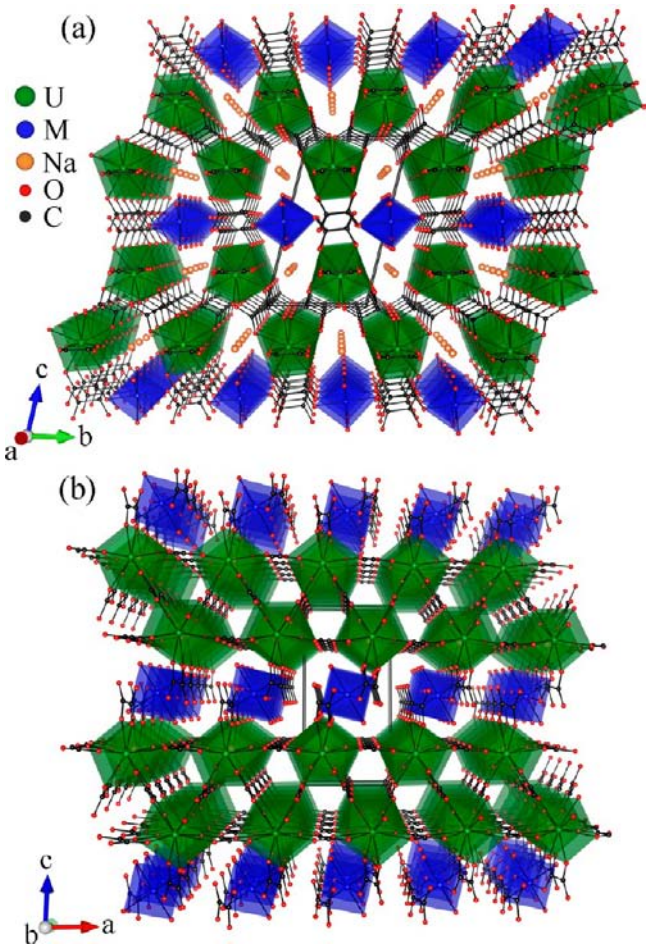

Figure 2. Polyhedral structure representation of $Na_2U_2M(C_2O_4)_6(H_2O)_4$ (M = Mn^{2+}, Fe^{2+}, Co^{2+}, and Zn^{2+}) along the (a) *a*- and (b) *b*-axis. The three-dimensional network consists of UO_{10} and MO_6 polyhedra bridged by oxalate groups. For clarity, the H atoms of water molecules attached to the M^{2+} cations are omitted.

cations are located in a 5-fold coordination environment with four oxygen atoms from four oxalates and the other oxygen atom from one water molecule. The Na−O bond distances range from 2.485(5) to 2.515(4) Å. The local coordination environment of each cation is shown in Figure 4. Bond valence sum calculations[32,33] resulted in values of 0.98−1.03 for Na^+, 1.94−1.97 for M^{2+}, and 3.91−3.94 for U^{4+}, which are all in good agreement with the expected values, as well as confirming the +4 oxidation state of U^{4+}.

There are three unique oxalate anions, of which two act as bidentate ligands and one as a terdentate ligand. The former connect the U^{4+} cations via a side-by-side bonding scheme, which is typically found in U^{4+} containing oxalate compounds and which creates an average U−U separation of 6.400 Å. The latter oxalate group links U^{4+} and a divalent cation, leaving one terminal oxygen atom that is not bonded to another cation. The cation connectivity is shown in Figure 5.

The reported materials exhibit several interesting structural features that result from the connectivity of the different cation polyhedra. For example, the layers located in the *ab*-plane contain U^{4+} cations that are bridged by the tetradentate bridging oxalate groups as shown in Figure 5. These layers are further connected through MO_6 polyhedra along the *c*-axis. One of the interesting structural features is the existence of

dx.doi.org/10.1021/ic3026733 | Inorg. Chem. 2013, 52, 2199−2207

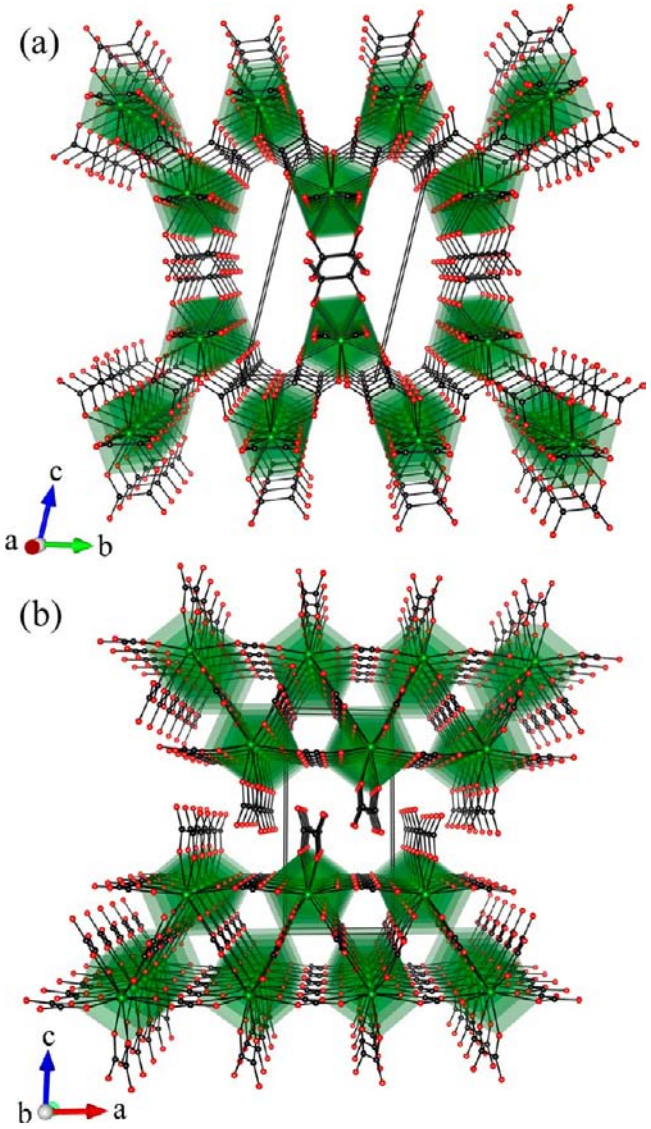

Figure 3. Polyhedral diagram of layers composed of the U^{4+} cations and oxalate anions for $Na_2U_2M(C_2O_4)_6(H_2O)_4$ (M = Mn^{2+}, Fe^{2+}, Co^{2+}, and Zn^{2+}) along the (a) *a*- and (b) *b*-axis are shown. For clarity, the M^{2+} cations and water molecules are omitted.

three-membered rings consisting of three uranium cations and three oxalate groups that run along the *a*- and *b*-axes. Of the known U^{4+} containing oxalates, only two other compounds, $U(C_2O_4)_2(H_2O)_x$ (x = 2 and 6),[15,26] exhibit the layer-type structure and contain UO_{10} and UO_8 polyhedra, respectively.

As stated earlier, the high coordination number is characteristic of actinide elements in low oxidation states. Studies based on the known hydration numbers in actinides suggest that the U^{4+} cation can possess a 10-fold coordination environment, while the other tetravalent actinide cations can only have a coordination number of up to nine.[34−36] As shown in Figure 4, the U^{4+} cation is in fact observed in UO_{10} polyhedra that are surrounded by five oxalate ligands. This structural motif is also found in other oxalates such as $(NH_4)_2U_2(C_2O_4)_5(H_2O)_{0.7}$[20] and α- and β-$K_4U(C_2O_4)_4(H_2O)_4$.[25] This coordination environment is potentially better defined as a sphenocorona rather than as a bicapped square pyramid.

The oxalate ligands bridge the UO_{10} and MO_6 polyhedra resulting in a three-dimensional network. In general, the oxalate ligand exhibits two bonding modes, one as a bidentate terminating and one as a tetradentate bridging ligand. As expected, the former is found in low-dimensional structures,[37,38] while the latter is observed in high-dimensional structures.[26,27] There are three unique oxalate groups in the reported materials. As shown in Figure 5, the two oxalate groups linking the U^{4+} cations act as tetradentate bridging ligands, while the other oxalate ligand between the U^{4+} and M^{2+} cations behaves as a terdentate ligand. In the known uranium oxalates it appears that the terdentate oxalate ligand motif is only found in $(NH_4)_2UO_2(C_2O_4)_2$,[20] which is a molecular compound containing the U^{6+} cation. $Na_2U_2M(C_2O_4)_6(H_2O)_4$ (M = Mn^{2+}, Fe^{2+}, Co^{2+}, and Zn^{2+}) is thus the first U^{4+} containing structural series to exhibit the bridging terdentate oxalate motif in an extended structure. It is expected that this bonding mode influences the C−O bond distances between bridging and terminal oxalate ligands. As seen in Table S5, the average C(3)−O(8) bond distance (1.218 Å) in a terminal position of the terdentate oxalate ligand is in fact slightly shorter than the average C−O distance (1.256 Å) in tetradentate bridging oxalate ligands.

Infrared Spectroscopy. The infrared spectra for the reported materials are very similar between 650 and 4000 cm^{-1} due to the fact that they are isostructural. The bands observed in the region 3200−3600 cm^{-1} are attributable to O−

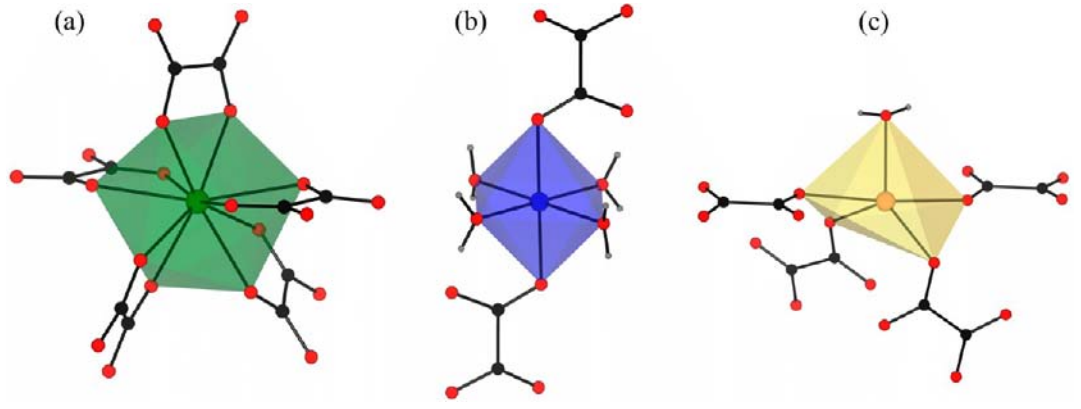

Figure 4. Local coordination environments of $Na_2U_2M(C_2O_4)_6(H_2O)_4$ (M = Mn^{2+}, Fe^{2+}, Co^{2+}, and Zn^{2+}). The U^{4+} cation is surrounded by five oxalate ligands (a), the M^{2+} cations are bonded to four water molecules and two oxalate groups (b), and the Na^+ cation is linked to one water molecule and four oxalate groups (c).

dx.doi.org/10.1021/ic3026733 | *Inorg. Chem.* 2013, 52, 2199−2207

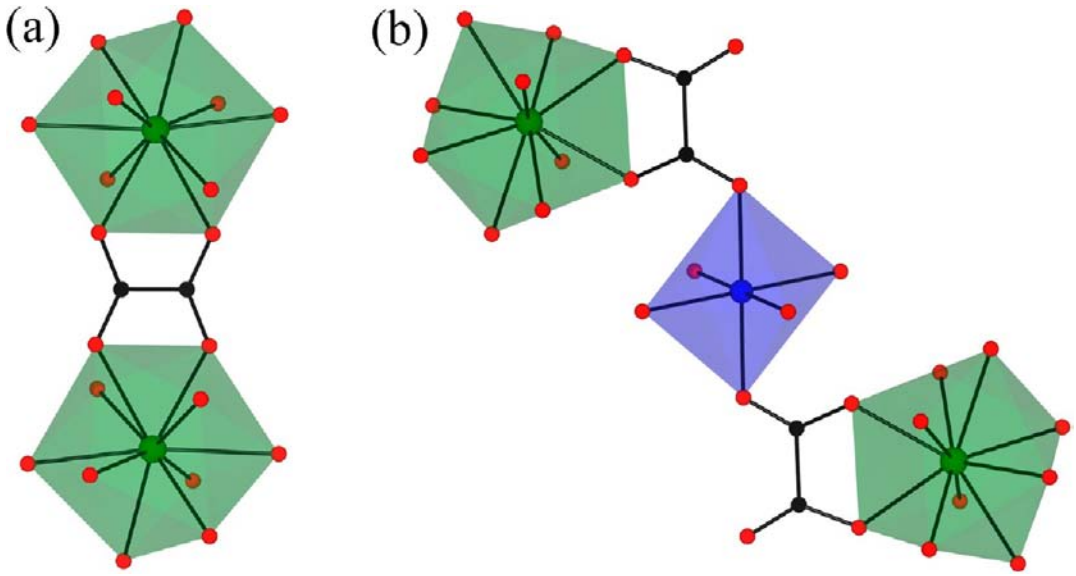

Figure 5. Connectivity between the U^{4+} cation and M^{2+} (M = Mn^{2+}, Fe^{2+}, Co^{2+}, and Zn^{2+}) cations. All four oxygen atoms in the oxalate ligand are bonded to two U^{4+} cations in part a, whereas in part b three oxygen atoms in the oxalate ligand are linked to the U^{4+} and M^{2+} cations leaving one oxygen atom in a terminal position. For the sake of clarity, the H atoms around the M^{2+} cation are omitted.

H vibrations in the water molecules. The bands found around 1600 cm^{-1} can be attributed to asymmetric stretching of C−O vibrations, whereas the bands observed in 1200−1450 cm^{-1} can be attributed to the symmetric stretching of C−O vibrations. The bands below 1000 cm^{-1} can be assigned to C−C, C−O−O, or metal−oxygen vibrations. The assignments are consistent with previously reported data.[39,40] The IR spectra are given in Figure S3.

UV−Vis Diffuse Reflectance Spectroscopy. UV−vis diffuse reflectance data were measured on ground crystals of all materials of the series, $Na_2U_2M(C_2O_4)_6(H_2O)_4$ (M = Mn^{2+}, Fe^{2+}, Co^{2+}, and Zn^{2+}). As seen in Figure 6, all spectra are similar except the iron containing uranate, where the broader absorption band is observed around 450 nm. For all spectra, it can be expected that the absorption bands are mainly attributed to the f−f transitions in the U^{4+} cation. It is likely that although d−d transitions in the divalent transition metal cations are present, the transitions are not clearly seen because the d−d transitions are weak and broader than the f−f transitions. The absorption bands above 400 nm are f−f transitions from the U^{4+} cations, which include transitions from the ground state of $^3H_4$ to the excited states such as $^1I_6$, $^3P_1$, $^1G_4$, $^1D_2$, $^3P_0$, $^3H_6$, $^3H_4$, etc., based on the energy level diagram for the U^{4+} cation.[41−43] The optical data therefore confirms the presence of the U^{4+} cation. The band gaps estimated by the onset of the absorption edge resulted in values of approximate 3.1 eV for $Na_2U_2M(C_2O_4)_6(H_2O)_4$ (M = Mn^{2+}, Co^{2+}, and Zn^{2+}), and 2.5 eV for $Na_2U_2Fe(C_2O_4)_6(H_2O)_4$, respectively, suggesting that they are semiconducting materials.

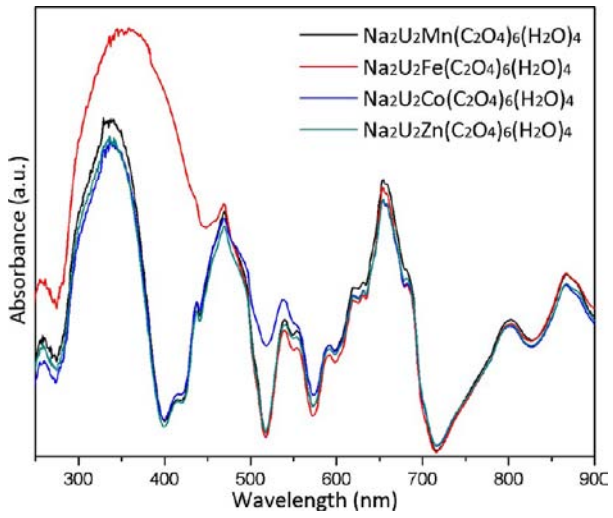

Figure 6. UV−vis diffuse reflectance spectra for $Na_2U_2Zn(C_2O_4)_6(H_2O)_4$ (M = Mn^{2+}, Fe^{2+}, Co^{2+}, and Zn^{2+}).

Thermal Analyses. The thermal behavior of the materials was investigated using thermogravimetric analysis (TGA) over the temperature range of RT to 1000 °C under nitrogen flow. TGA data are shown in Figures S4 and S5. The first observed weight loss starts at approximately 200 °C due to the loss of waters of hydration. This weight loss continues as the temperature is increased to 900 °C and includes the decomposition of the oxalate groups. The experimental weight losses of 42.5%, 43.1%, 43.9%, and 46.4% are in good agreement with the calculated weight losses of 42.8%, 42.8%, 42.7%, and 42.5%, for Mn, Fe, Co, and Zn containing uranates, respectively. The final residues, based on a powder X-ray diffraction analysis, are $NaUO_3$,[44] UO_2,[45] and MnO[46] in the case of $Na_2U_2Mn(C_2O_4)_6(H_2O)_4$; $NaUO_3$,[44] UO_2,[45] and an unidentified phases in the case of $Na_2U_2Fe(C_2O_4)_6(H_2O)_4$ and $Na_2U_2Co(C_2O_4)_6(H_2O)_4$; and $NaUO_3$,[44] $Na_2U_2O_7$,[47] and ZnO[48] in the case of $Na_2U_2Zn(C_2O_4)_6(H_2O)_4$. For all compounds, the residues contain U^{5+} and U^{6+} containing products, indicating that a redox reaction occurred during the decomposition process. An additional thermal analysis using 5% H_2 gas was performed on $Na_2U_2Zn(C_2O_4)_6(H_2O)_4$ to see if the outcome under hydrogen was different from what was observed using nitrogen. It turned out that the overall result is almost the same, as shown in Figure S4; however, the ZnO residue was no longer evident, as it was presumably reduced to the metal.

Magnetic Properties. The $Na_2U_2M(C_2O_4)_6(H_2O)_4$ (M = Mn^{2+}, Fe^{2+}, Co^{2+}, and Zn^{2+}) system is convenient for studying

dx.doi.org/10.1021/ic3026733 | Inorg. Chem. 2013, 52, 2199−2207

the magnetic properties of U^{4+} and its interactions with magnetic divalent transition elements. The U^{4+} (f^2) cation has two unpaired f-electrons that will contribute to the magnetic properties, and the transition metal cations Mn^{2+}(d^5), Fe^{2+}(d^6), and Co^{2+}(d^7) have d-electrons that also will play a role; only zinc is nonmagnetic in this series. This allows us to investigate the contribution to the magnetic susceptibility of only uranium in $Na_2U_2Zn(C_2O_4)_6(H_2O)_4$, and the combined contributions of uranium and manganese, cobalt and iron in $Na_2U_2M(C_2O_4)_6(H_2O)_4$ (M = Mn^{2+}, Fe^{2+}, and Co^{2+}), respectively.

The temperature dependence of the magnetic susceptibility for $Na_2U_2Zn(C_2O_4)_6(H_2O)_4$, reflecting only the contribution of U^{4+}, in an applied field of 1000 Oe is shown in Figure 7. No

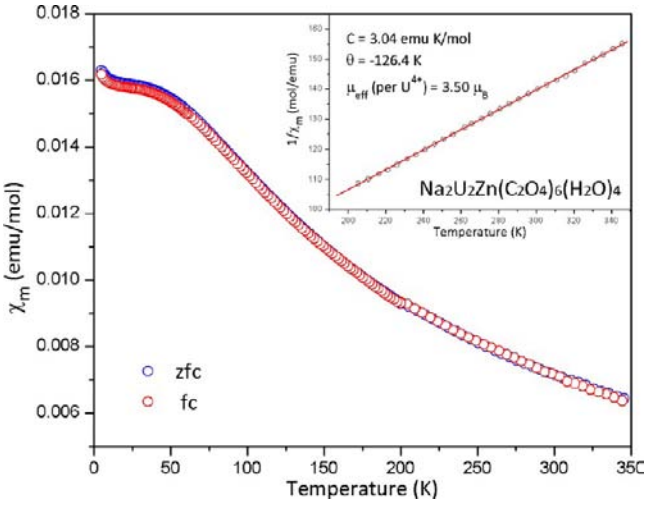

Figure 7. Temperature dependence of the molar magnetic susceptibility, χ_m, of $Na_2U_2Zn(C_2O_4)_6(H_2O)_4$ measured in an applied field of 1000 Oe. Inset shows the inverse susceptibility vs temperature plot with fit to the Curie–Weiss law.

differences are observed between the zero field cooled (zfc) and field cooled (fc) data. The inverse susceptibility versus temperature plot is shown in the inset. The susceptibility data were fit to the Curie–Weiss law, $\chi = C/(T - \theta)$, in the linear temperature range 200–350 K, where C is the Curie constant and θ is the paramagnetic Weiss constant. The constants extracted from the curve fitting are summarized in Table 3. On the basis of the fit, the U^{4+} cation gives a magnetic moment of 3.50 μ_B, in good agreement with the expected value of 3.58 μ_B, calculated using the Russell–Saunders coupling scheme ($g_J = {}^4/_5$ and $J = 4$) for a $^3H_4$ ground state. As seen in Figure 7, the magnetization increases gradually with decreasing temperature, and temperature independent behavior is found below around 5 K indicating that excited states are not

Table 3. Constants Extracted from the Magnetic Susceptibility Data for $Na_2U_2M(C_2O_4)_6(H_2O)_4$ (M = Mn^{2+}, Fe^{2+}, Co^{2+}, and Zn^{2+})[a]

	C (emu K mol^{-1})	Θ (K)	μ_{eff}/μ_B
$Na_2U_2Mn(C_2O_4)_6(H_2O)_4$	7.68	−30.1	6.01
$Na_2U_2Fe(C_2O_4)_6(H_2O)_4$	6.90	−26.7	5.46
$Na_2U_2Co(C_2O_4)_6(H_2O)_4$	6.37	−51.8	5.06
$Na_2U_2Zn(C_2O_4)_6(H_2O)_4$	3.04	−126.4	3.50

[a] C, Θ, and μ_{eff} represent the Curie constant, the Weiss constant, and effective magnetic moment, respectively.

thermally accessible at the low temperature. Figure 8 shows temperature dependence of the $\chi_m T$ data. The $\chi_m T$ value drops

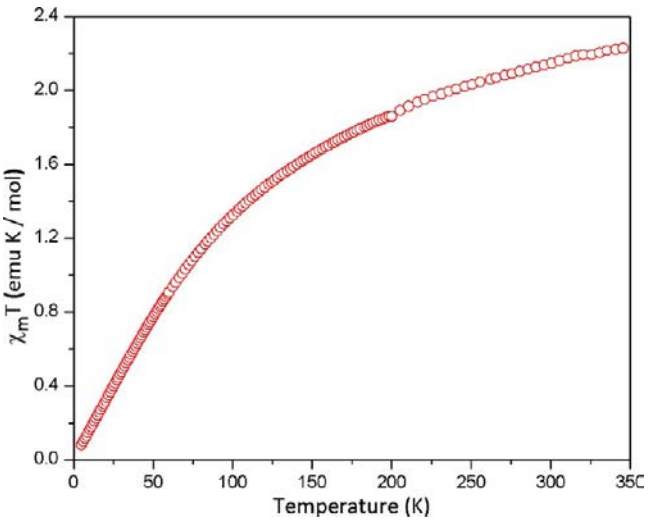

Figure 8. Plot of $\chi_m T$ vs temperature for $Na_2U_2Zn(C_2O_4)_6(H_2O)_4$. Data were collected in an applied field of 1000 Oe.

off gradually with decreasing temperature, indicating the existence of antiferromagnetic interactions, which are consistent with the negative Weiss constant of −126.4 K from the curve fitting in the high temperature region. Below around 100 K, however, the values of $\chi_m T$ decrease rapidly and tend toward zero with a minimum value of 0.082 emu K mol^{-1} (μ_{eff} = 0.81 μ_B) at 5 K. This is likely due to the presence of a zero-field splitting and contribution of a singlet ground state of the U^{4+}cation at low temperature, which is also observed in several known materials containing the U^{4+} cation.[14,49−52]

The temperature dependence of the magnetic susceptibility data for $Na_2U_2M(C_2O_4)_6(H_2O)_4$ (M = Mn^{2+}, Fe^{2+}, and Co^{2+}) in an applied field of 1000 Oe are shown in Figures 9–11. The magnetic properties of the three materials are similar to each other, but quite different from that of $Na_2U_2Zn(C_2O_4)_6(H_2O)_4$,

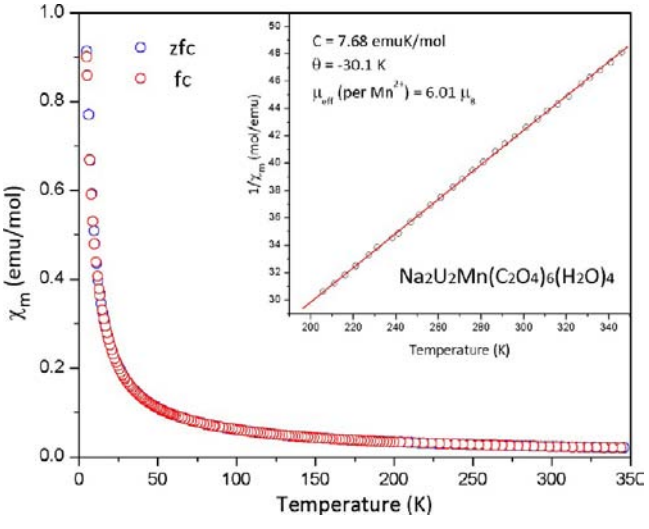

Figure 9. Temperature dependence of the molar magnetic susceptibility, χ_m, of $Na_2U_2Mn(C_2O_4)_6(H_2O)_4$ measured in an applied field of 1000 Oe. Inset shows the inverse susceptibility vs temperature plot with fit to the Curie–Weiss law.

dx.doi.org/10.1021/ic3026733 | Inorg. Chem. 2013, 52, 2199–2207

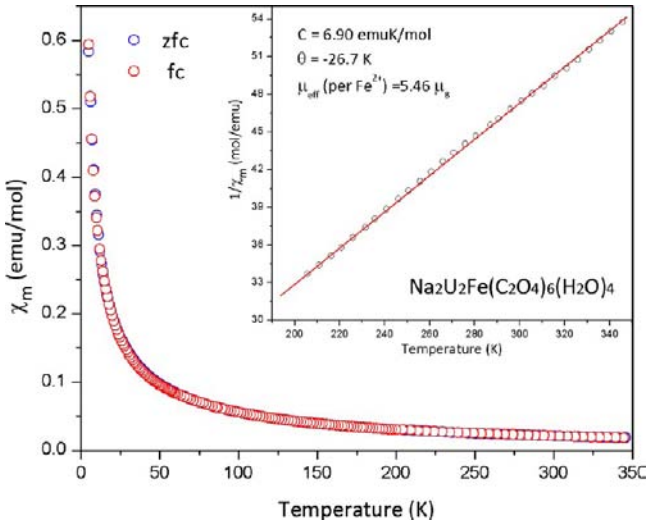

Figure 10. Temperature dependence of the molar magnetic susceptibility, χ_m, of $Na_2U_2Fe(C_2O_4)_6(H_2O)_4$ measured in an applied field of 1000 Oe. Inset shows the inverse susceptibility vs temperature plot with fit to the Curie–Weiss law.

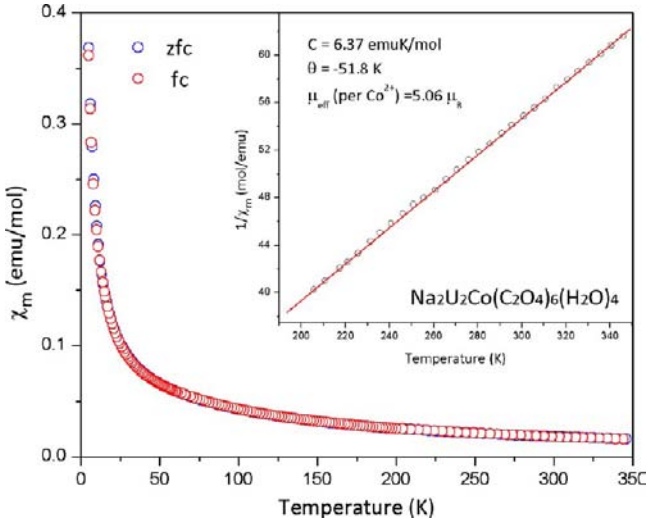

Figure 11. Temperature dependence of the molar magnetic susceptibility, χ_m, of $Na_2U_2Co(C_2O_4)_6(H_2O)_4$ measured in an applied field of 1000 Oe. Inset shows the inverse susceptibility vs temperature plot with fit to the Curie–Weiss law.

attributable to the presence of the magnetic Mn^{2+}, Fe^{2+}, and Co^{2+} cations in the structure. As seen in Figures 9–11, the magnetizations increase gradually as the temperature decreases; however, the magnetizations increase rapidly below around 50 K. The values obtained from the curve fitting to the Curie–Weiss law in the high temperature range (200 K < T < 350 K) are summarized in Table 3, where the effective magnetic moments are close to the usually observed values of 5.9, 5.1–5.5, and 4.1–5.2 μ_B for Mn^{2+}, Fe^{2+}, and Co^{2+}, respectively. In this case, the theoretical magnetic moment of 3.58 μ_B for U^{4+} was used to obtain the experimental magnetic moments of the divalent cations. Conversely, the magnetic moment of the U^{4+} cation can be calculated from the $Na_2U_2Mn(C_2O_4)_6(H_2O)_4$ data when using a moment of μ_{eff} = 5.92 μ_B for Mn^{2+}, resulting in a value of 3.65 μ_B for U^{4+}, which is slightly larger than the expected value of (3.58 μ_B) and the observed value of (3.50 μ_B) in the Zn containing uranate.

The $\chi_m T$ versus T data are shown in Figure 12. For all materials, the $\chi_m T$ values decrease gradually with decreasing

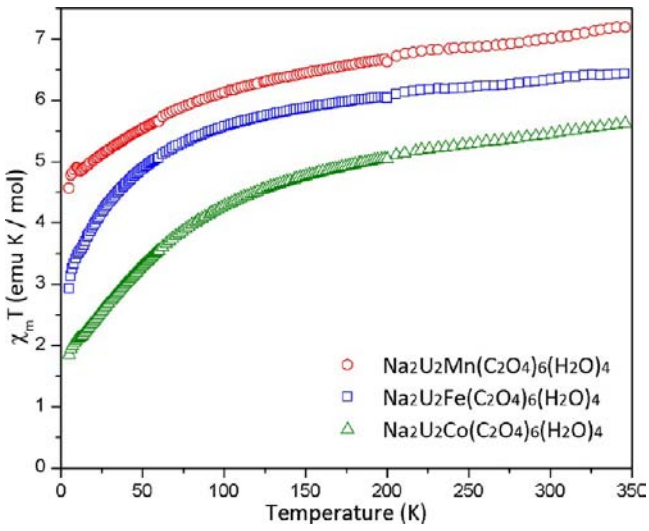

Figure 12. Plot of $\chi_m T$ vs temperature for $Na_2U_2M(C_2O_4)_6(H_2O)_4$ (M = Mn^{2+}, Fe^{2+}, and Co^{2+}). Data were collected in an applied field of 1000 Oe.

temperature. This indicates that the presence of antiferromagnetic interactions, which are consistent with the negative Weiss constants of −30.1, −26.7, and −51.8 K for the Mn, Fe, and Co containing uranates, respectively. The high temperature values of $\chi_m T$ result from the combined contributions of the M^{2+} and U^{4+} cations. At 5 K, however, the $\chi_m T$ values are 4.56 (6.05 μ_B), 2.92(4.85 μ_B), and 1.84 (3.85 μ_B) emu K mol^{-1}, which are close to the expected spin-only values of 4.36 (5.92 μ_B), 2.98 (4.90 μ_B), and 1.86 (3.87 μ_B) emu K mol^{-1} for Mn^{2+}, Fe^{2+}, and Co^{2+}, respectively. This is consistent with the $\chi_m T$ data for $Na_2U_2Zn(C_2O_4)_6(H_2O)_4$ shown in Figure 8, where the negligible magnetic contributions of the U^{4+} cation is found at 5 K. For this reason, the contribution from the divalent cations dominates the magnetic moments at low temperature. This is consistent with the local ground state of the U^{4+} magnetic center at low temperatures being a singlet state. For all of the reported materials, although local antiferromagnetic interactions were expected on the basis of the negative Weiss constants, no long-range transitions were observed down to 5 K. This is not unexpected because the magnetic cations, U^{4+} and divalent cations, are bridged by oxalate groups, which results in relatively long metal–metal separations of over 5 and 6 Å for U^{4+}–M^{2+} and U^{4+}–U^{4+}, respectively.

CONCLUSIONS

We have successfully synthesized and characterized new reduced uranium oxalates, $Na_2U_2M(C_2O_4)_6(H_2O)_4$ (M = Mn^{2+}, Fe^{2+}, Co^{2+}, and Zn^{2+}). The isostructural materials exhibit a three-dimensional crystal structure consisting of UO_{10} and MO_6 polyhedra bridged by oxalate groups. The magnetic behavior of the U^{4+} cation was investigated in $Na_2U_2Zn(C_2O_4)_6(H_2O)_4$ and found to exhibit temperature independent behavior at low temperature. The effective magnetic moment of 3.50 μ_B for the U^{4+} cation was obtained from the high temperature data. At low temperatures the magnetic moment tended toward zero, consistent with the ground state of the U^{4+} cation being a singlet state. For the other materials, the

dx.doi.org/10.1021/ic3026733 | Inorg. Chem. 2013, 52, 2199–2207

magnetization increased rapidly at low temperature, and exhibited local antiferromagnetic interactions.

■ ASSOCIATED CONTENT

Supporting Information

X-ray data in CIF format, powder XRD patterns, IR and UV−vis spectra, TGA diagrams, and atomic coordinates and equivalent isotropic displacement parameters. This material is available free of charge via the Internet at http://pubs.acs.org.

■ AUTHOR INFORMATION

Corresponding Author

*E-mail: zurloye@mailbox.sc.edu.

Notes

The authors declare no competing financial interest.

■ ACKNOWLEDGMENTS

Research supported by the U.S. Department of Energy, Office of Basic Energy Sciences, Division of Materials Sciences and Engineering under Award DE-SC0008664.

■ REFERENCES

(1) Yamaji, A.; Nakano, Y.; Uchikawa, S.; Okubo, T. *Nucl. Technol.* **2012**, *179*, 309.
(2) Kim, K.-T. *J. Nucl. Mater.* **2010**, *404*, 128.
(3) Oji, L. N.; Martin, K. B.; Stallings, M. E.; Duff, M. C. *Nucl. Technol.* **2006**, *154*, 237.
(4) Jackson, J. M.; Burns, P. C. *Can. Mineral.* **2001**, *39*, 187.
(5) Burns, P. C.; Olson, R. A.; Finch, R. J.; Hanchar, J. M.; Thibault, Y. *J. Nucl. Mater.* **2000**, *278*, 290.
(6) Shannon, R. D.; Prewitt, C. T. *Acta Crystallogr., Sect. B* **1969**, *25*, 925.
(7) Liu, H.-K.; Chang, W.-J.; Lii, K.-H. *Inorg. Chem.* **2012**, *50*, 11773.
(8) Diwu, J.; Albrecht-Schmitt, T. E. *Inorg. Chem.* **2012**, *51*, 4432.
(9) Chen, C.-L.; Nguyen, Q. B.; Chen, C.-S.; Lii, K.-H. *Inorg. Chem.* **2012**, *51*, 7463.
(10) Nguyen, Q.-B.; Lii, K.-H. *Inorg. Chem.* **2011**, *50*, 9936.
(11) Nguyen, Q. B.; Liu, H.-K.; Chang, W.-J.; Lii, K.-H. *Inorg. Chem.* **2011**, *50*, 4241.
(12) Liu, H.-K.; Lii, K.-H. *Inorg. Chem.* **2011**, *50*, 5870.
(13) Lin, C.-H.; Lii, K.-H. *Angew. Chem., Int. Ed.* **2008**, *47*, 8711.
(14) Lai, Y.-L.; Chiang, R.-K.; Lii, K.-H.; Wang, S.-L. *Chem. Mater.* **2008**, *20*, 523.
(15) Grinbergs, A.; Petrzhak, G. I.; Lozhkina, G. S.; Karago, L. V. *Radiokhimiya* **1972**, *14*, 397.
(16) Andreev, G.; Budantseva, N.; Fedoseev, A.; Moisy, P. *Inorg. Chem.* **2011**, *50*, 11481.
(17) Serezhkina, L. B.; Peresypkina, E. V.; Neklyudova, N. A.; Virovets, A. V. *Crystallogr. Rep.* **2010**, *55*, 769.
(18) Alcock, N. W. *J. Chem. Soc., Dalton Trans.* **1973**, 1616.
(19) Artem'eva, M. Y.; Vologzhanina, A. V.; Dolgushin, F. M.; Antipin, M. Y.; Serezhkina, L. B.; Serezhkin, V. N. *Zh. Neorg. Khim.* **2004**, *49*, 2068.
(20) Alcock, N. W. *J. Chem. Soc., Dalton Trans.* **1973**, 1610.
(21) Duvieubourg-Garela, L.; Vigier, N.; Abraham, F.; Grandjean, S. *J. Solid State Chem.* **2008**, *181*, 1899.
(22) Art'emeva, M. Y.; Mikhailov, Y. N.; Gorbunova, Y. E.; Serezhkina, L. B.; Serezhkin, V. N. *Zh. Neorg. Khim.* **2003**, *48*, 1470.
(23) Chapelet-Arab, B.; Nowogrocki, G.; Abraham, F.; Grandjean, S. *J. Solid State Chem.* **2005**, *178*, 3046.
(24) Moertl, K. P.; Sutter, J.-P.; Golhen, S.; Ouahab, L.; Kahn, O. *Inorg. Chem.* **2000**, *39*, 1626.
(25) Favas, M. C.; Kepert, D. L.; Patrick, J. M.; White, A. H. *J. Chem. Soc., Dalton Trans.* **1983**, 571.
(26) Clavier, N.; Hingant, N.; Rivenet, M.; Obbade, S.; Dacheux, N.; Barre, N.; Abraham, F. *Inorg. Chem.* **2010**, *49*, 1921.
(27) Wang, C.-M.; Liao, C.-H.; Chen, P.-L.; Lii, K.-H. *Inorg. Chem.* **2006**, *45*, 1436.
(28) Imaz, I.; Bravic, G.; Sutter, J.-P. *Chem. Commun.* **2005**, 993.
(29) Spirlet, M. R.; Rebizant, J.; Kanellakopulos, B.; Dornberger, E. *J. Less-Common Met.* **1986**, *122*, 205.
(30) *SMART Version 5.625, SAINT+ Version 6.45, and SADABS Version 2.05*; Bruker Analytical X-ray Systems, Inc.: Madison, WI, 2001.
(31) *SHELXTL Version 6.14*; Bruker Analytical X-ray Systems, Inc.: Madison, WI, 2000.
(32) Brese, N. E.; O'Keeffe, M. *Acta Crystallogr.* **1991**, *B47*, 192.
(33) Brown, I. D.; Altermatt, D. *Acta Crystallogr.* **1985**, *B41*, 244.
(34) Torapava, N.; Persson, I.; Eriksson, L.; Lundberg, D. *Inorg. Chem.* **2009**, *48*, 11712.
(35) Ikeda-Ohno, A.; Hennig, C.; Rossberg, A.; Funke, H.; Scheinost, A. C.; Bernhard, G.; Yaita, T. *Inorg. Chem.* **2008**, *47*, 8294.
(36) Moll, H.; Denecke, M. A.; Jalilehvand, F.; Sandstroem, M.; Grenthe, I. *Inorg. Chem.* **1999**, *38*, 1795.
(37) Mikhailov, Y. N.; Gorbunova, Y. E.; Shishkina, O. V.; Serezhkina, L. B.; Serezhkin, V. N. *Zh. Neorg. Khim.* **2000**, *45*, 1825.
(38) Elovskikh, N. N.; Rumyantseva, K. T. *Zh. Neorg. Khim.* **1962**, *7*, 2639.
(39) Trpkovska, M.; Soptrajanov, B.; Pejov, L. *Glas. Hem. Tehnol. Maked.* **2002**, *21*, 111.
(40) Scott, K. L.; Wieghardt, K.; Sykes, A. G. *Inorg. Chem.* **1973**, *12*, 655.
(41) Binnemans, K.; Couwenberg, I.; De, L. H.; Gorller-Walrand, C.; Adam, J. L. *J. Alloys Compd.* **1999**, *285*, 105.
(42) Carnall, W. T.; Liu, G. K.; Williams, C. W.; Reid, M. F. *J. Chem. Phys.* **1991**, *95*, 7194.
(43) Krupa, J. C. *Inorg. Chim. Acta* **1987**, *139*, 223.
(44) Chippindale, A. M.; Dickens, P. G.; Harrison, W. T. A. *J. Solid State Chem.* **1989**, *78*, 256.
(45) Macdonald, J. E.; Clausen, K.; Garrard, B.; Hackett, M. A.; Hayes, W.; Osborn, R.; Schnabel, P.; Hutchings, M. T. *High Temp.−High Pressures* **1985**, *17*, 27.
(46) Sasaki, S.; Fujino, K.; Takeuchi, Y. *Proc. Jpn. Acad., Ser. B* **1979**, *55*, 43.
(47) Gasperin, M. *J. Less-Common Met.* **1986**, *119*, 83.
(48) Lucas, L. N. D. *Proc. Phys. Soc., London* **1951**, *64A*, 943.
(49) Siladke, N. A.; Meihaus, K. R.; Ziller, J. W.; Fang, M.; Furche, F.; Long, J. R.; Evans, W. J. *J. Am. Chem. Soc.* **2011**, *134*, 1243.
(50) Nocton, G.; Pecaut, J.; Mazzanati, M. *Angew. Chem., Int. Ed.* **2008**, *47*, 3040.
(51) Schelter, E. J.; Morris, D. E.; Scott, B. L.; Thompson, J. D.; Kiplinger, J. L. *Inorg. Chem.* **2007**, *46*, 5528.
(52) Evans, W. J.; Miller, K. A.; Ziller, J. W.; Greaves, J. *Inorg. Chem.* **2007**, *46*, 8008.